The structural and chemical origin of the oxygen redox activity in layered and cation-disordered Li-excess cathode materials

Dong-Hwa Seo[1,2†], Jinhyuk Lee[1,2†], Alexander Urban[2], Rahul Malik[1], ShinYoung Kang[1] and Gerbrand Ceder[1,2,3]*

Lithium-ion batteries are now reaching the energy density limits set by their electrode materials, requiring new paradigms for Li$^+$ and electron hosting in solid-state electrodes. Reversible oxygen redox in the solid state in particular has the potential to enable high energy density as it can deliver excess capacity beyond the theoretical transition-metal redox-capacity at a high voltage. Nevertheless, the structural and chemical origin of the process is not understood, preventing the rational design of better cathode materials. Here, we demonstrate how very specific local Li-excess environments around oxygen atoms necessarily lead to labile oxygen electrons that can be more easily extracted and participate in the practical capacity of cathodes. The identification of the local structural components that create oxygen redox sets a new direction for the design of high-energy-density cathode materials.

Over the past two decades, lithium-ion battery technology has contributed greatly to human progress and enabled many of the conveniences of modern life by powering increasingly capable portable electronics[1]. However, with the increasing complexity of technology comes a demand for batteries with higher energy density, which thus leads to a requirement for cathode materials with higher energy densities[2–4].

The traditional design paradigm for Li-ion battery cathodes has been to create compounds in which the amount of extractable Li$^+$ is well balanced with an oxidizable transition metal (TM) species (such as Mn, Fe, Co or Ni) to provide the charge-compensating electrons, all contained in an oxide or sulfide host. Transition metals have been considered the sole sources of electrochemical activity in an intercalation cathode, and as a consequence the theoretical specific capacity is limited by the number of electrons that the transition-metal ions can exchange per unit mass[5–9]. Recent observations have brought this simple picture into question and argued that oxygen ions in oxide cathodes may also participate in the redox reaction. This oxygen redox is often ascribed to covalency, following theoretical[10,11] and experimental[12–16] work in the last two decades that has demonstrated large electron density changes on oxygen when the transition metal is oxidized. However, covalency cannot lead to a higher capacity than would be expected from the transition metal alone, as the number of transition-metal orbitals remains unchanged when they hybridize with the oxygen ligands. The more important argument for the future of the Li-ion battery field is whether oxygen oxidation can create extra capacity beyond what is predicted from the transition-metal content alone, as has been argued for several Li-excess materials, such as $Li_{1.2}Ni_{0.2}Mn_{0.6}O_2$, $Li_2Ru_{0.5}Sn_{0.5}O_2$ and $Li_{1.3}Mn_{0.4}Nb_{0.3}O_2$ (refs 3,17,18).

In this Article, we use *ab initio* calculations to demonstrate which specific chemical and structural features lead to electrochemically active oxygen states in cathode materials. Our results uncover a specific atomistic origin of oxygen redox and explain why this oxygen capacity is so often observed in Li-excess materials and why it is observed with some metals and not with others. The specific nature of our findings reveals a clear and exciting path towards creating the next generation of cathode materials with substantially higher energy density than current cathode materials.

Results and discussion

Appearance of labile oxygen states in Li metal oxides. It is generally understood that the relative energy of the TM versus oxygen states determines which species (TM versus O) are oxidized upon delithiation[1,19]. As the energy level of those states depends on the species in a compound and their chemical bonding, local environments in a crystal structure can play a critical role in the redox processes and the participation of oxygen in them[10]. Unlike in conventional stoichiometric layered cathode materials, which are well ordered and in which only a single local environment exists for oxygen ions, a variety of local oxygen environments exist in Li-excess materials or materials with cation disorder. By systematically calculating and analysing the density of states (DOS) and charge/spin density around oxygen ions in various local environments using density functional theory (DFT) (ref. 20), we demonstrate that the Li-excess content and the local configuration sensitively affect oxygen redox activity in the oxide cathodes. To accurately study the oxygen redox activity, all calculations were performed with DFT using the Heyd–Scuseria–Ernzerhof (HSE06) hybrid functional[21], which can correct the self-interaction errors (SIEs) for both metal (M) and O atoms. Note that the generalized gradient approximation (GGA) and GGA+U, which are frequently used in DFT calculations, cannot properly predict the oxygen redox activity, because they cannot correct the SIE for O atoms[22].

We start with $LiNiO_2$ (containing site disorder) and Li_2MnO_3 as two simple model systems before moving on to more complex materials. $LiNiO_2$ is one of the most studied materials and Ni is the dominant redox active species in many technologically important cathodes such as $LiNi_{1/3}Mn_{1/3}Co_{1/3}O_2$ and $LiNi_{0.8}Co_{0.15}Al_{0.05}O_2$ (refs 23,24). In perfectly layered $LiNiO_2$, oxygen ions are exclusively

[1]Department of Materials Science and Engineering, Massachusetts Institute of Technology, Cambridge, Massachusetts 02139, USA. [2]Department of Materials Science and Engineering, UC Berkeley, Berkeley, California 94720, USA. [3]Materials Science Division, Lawrence Berkeley National Laboratory, Berkeley, California 94720, USA. †These authors contributed equally to this work. *e-mail: gceder@berkeley.edu
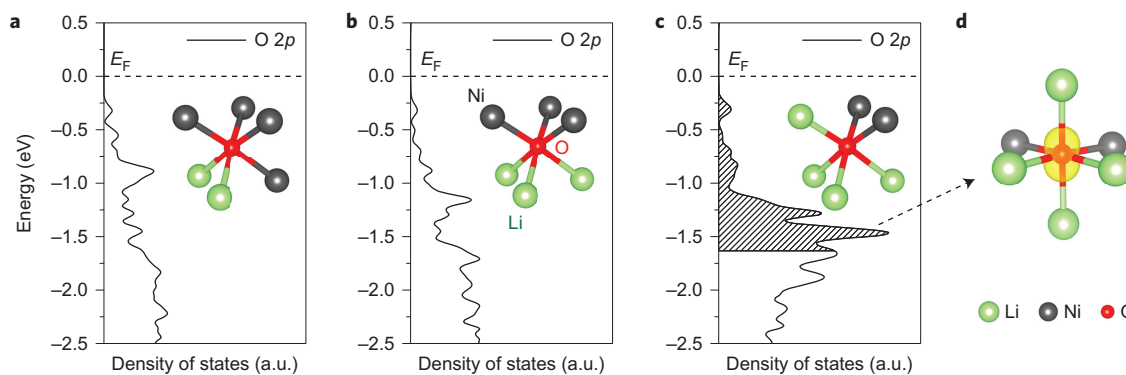
Figure 1 | Effect of local atomic environments on the electronic states of O ions in cation-mixed layered LiNiO₂. Cation mixing introduces various local environments around oxygen. **a–c**, Projected density of states (pDOS) of the O 2p orbitals of O atoms in cation-mixed layered LiNiO$_2$ coordinated by two Li and four Ni (**a**), three Li and three Ni (**b**) and four Li and two Ni (**c**). Insets: coordination of the O ion. **d**, Isosurface of the charge density (yellow) around the oxygen coordinated by four Li and two Ni (**c**), in the energy range of 0 to −1.64 eV. Increased pDOS can be found near the Fermi level for the O ion coordinated by four Li and two Ni, which originates from the particular Li–O–Li configuration.

coordinated by three Li and three Ni (Fig. 1b). The other two environments in Fig. 1 are created by Li/Ni exchange (anti-sites): two Li and four Ni (Fig. 1a) and four Li and two Ni (Fig. 1c).

The projected DOS (pDOS) of the oxygen 2p states of the three oxygen environments are shown in Fig. 1a–c. Although there is not much change in the oxygen pDOS between the 4Ni/2Li and 3Ni/3Li configurations, the oxygen pDOS changes substantially when four Li ions are near the oxygen (Fig. 1c). In particular, a much greater pDOS between 0 and −2.5 eV of the Fermi level is found for the oxygen ion coordinated with four Li and two Ni ions (Fig. 1c). The origin of this increased DOS can be identified by visualizing the charge density around the oxygen ion for the energy range between 0 and −1.64 eV (Fig. 1d). This energy range corresponds to the extraction of one electron per LiNiO$_2$. As seen in the isosurface plot, a large charge density resembling the shape of an isolated O 2p orbital is present along the direction where oxygen is linearly bonded to two Li (Li–O–Li configuration). This result indicates that the labile electrons from the O ion in the local Li-excess environment originate from this particular Li–O–Li configuration. This state has moved up from the bonding O 2p manifold of states at lower energies.

In many of the new exciting cathode materials[2,3,18,25], Li-excess is created by the substitution of some (transition) metals by Li, necessarily leading to more Li–O–Li configurations and, as a consequence, more potentially labile oxygen electrons (Supplementary Fig. 7). To confirm this hypothesis, we studied the oxygen electronic states in Li$_2$MnO$_3$ in which all O ions are in a local Li-excess environment containing a Li–O–Li configuration (Fig. 2a)[26,27].

Figure 2b presents pDOS from the O 2p orbitals and the Mn 3d orbitals in Li$_2$MnO$_3$. A much larger pDOS originates from the oxygen states than from the manganese states between 0 and −2.5 eV. The corresponding charge density plot around the O ion within 0 to −0.9 eV again resembles an oxygen p orbital along the Li–O–Li axis (Fig. 2c), confirming that the oxygen orbital along the Li–O–Li configuration contributes to the large oxygen pDOS close to the Fermi level. Within 0 to −0.9 eV, roughly two electrons per Li$_2$MnO$_3$ can be extracted. Oxygen oxidation in this compound is consistent with theoretical work in the literature[26,27]. To summarize, the Li–O–Li configuration introduces labile oxygen electrons in Li$_2$MnO$_3$, as in the case of the partially cation-mixed LiNiO$_2$.

Oxygen charge transfer from the labile oxygen states in Li-excess cathode materials. With the basic ideas in hand of how labile oxygen states can be created, we investigated more complex Li-excess compounds in which extra redox capacity beyond the theoretical TM-redox capacity has been observed: Li(Li/Mn/M)O$_2$

(M = Ni, Co, and so on) and Li$_2$Ru$_{0.5}$Sn$_{0.5}$O$_3$ are layered Li-excess materials[17,28], and Li$_{1.25}$Mn$_{0.5}$Nb$_{0.25}$O$_2$ (≈ Li$_{1.3}$Mn$_{0.4}$Nb$_{0.3}$O$_2$) and Li$_{1.2}$Ni$_{1/3}$Ti$_{1/3}$Mo$_{2/15}$O$_2$ are cation-disordered Li-excess materials[18,29,30]. For each of the compounds we constructed unit cells that take into account as much as is known about the structures. Fragments of these unit cells are shown in the top row of Fig. 3 (for more details see Supplementary Section 'Preparation of the structure models'). All compounds were delithiated beyond the conventional limit from TM redox.

Figure 3a–d plots the isosurface of the spin density around oxygen in partially delithiated Li$_{1.17−x}$Ni$_{0.25}$Mn$_{0.58}$O$_2$ ($x = 0.5$, 0.83), Li$_{2−x}$Ru$_{0.5}$Sn$_{0.5}$O$_3$ ($x = 0.5$, 1.5), Li$_{1.17−x}$Ni$_{0.33}$Ti$_{0.42}$Mo$_{0.08}$O$_2$ ($x = 0.5$, 0.83) and Li$_{1.25−x}$Mn$_{0.5}$Nb$_{0.25}$O$_2$ ($x = 0.75$, 1.0), respectively. To simplify the presentation, the spin densities around metal ions are not drawn in the figures. In all cases, we observe a large spin density from the oxygen ions along the Li–O–Li configuration with the shape of an isolated O 2p orbital, indicating a hole along the Li–O–Li configuration. These holes along the Li–O–Li configurations increase in number and density upon delithiation. As a hole on an O ion is direct evidence of oxygen oxidation[31], these results demonstrate that extraction of the labile oxygen electrons along the Li–O–Li configuration is the origin of oxygen oxidation and extra capacity beyond the TM redox capacity. Note that in the partially delithiated Li$_{1.17−x}$Ni$_{0.33}$Ti$_{0.42}$Mo$_{0.08}$O$_2$, one of the oxidized oxygens with the Li–O–Li configuration is not in a local Li-excess environment (Fig. 3c). This oxygen is coordinated with three TM (two Ni, one Ti) and three Li, but it still has the Li–O–Li configuration because of local cation disorder (Supplementary Fig. 7). In Li$_{0.5}$Ru$_{0.5}$Sn$_{0.5}$O$_3$, we observe a weak σ bond between two of the oxidized O ions (blue dashed oval) and an accompanying small rotation of their Li–O–Li axes (Supplementary Fig. 8). This is consistent with the experimental finding of O–O bonds (peroxo-like species) in the compound at high delithiation[3]. The conditions under which oxygen hole formation leads to peroxo-like bonds are discussed in more detail in the section 'Conditions for peroxo-like O–O bond formation' and in Supplementary Figs 8 and 9.

So far, we have established that the Li–O–Li configuration, either as a result of excess Li or cation disorder, gives rise to the labile oxygen electrons that participate in redox activity. In the following, we will unravel the structural and chemical origin of this phenomenon and show how, through the judicious choice of (transition) metal chemistry, it can be modified and controlled.

Origin of the labile oxygen states and their redox processes. In stoichiometric well-layered Li metal oxides, such as LiCoO$_2$, all O ions are coordinated by exactly three metal (M) ions and three
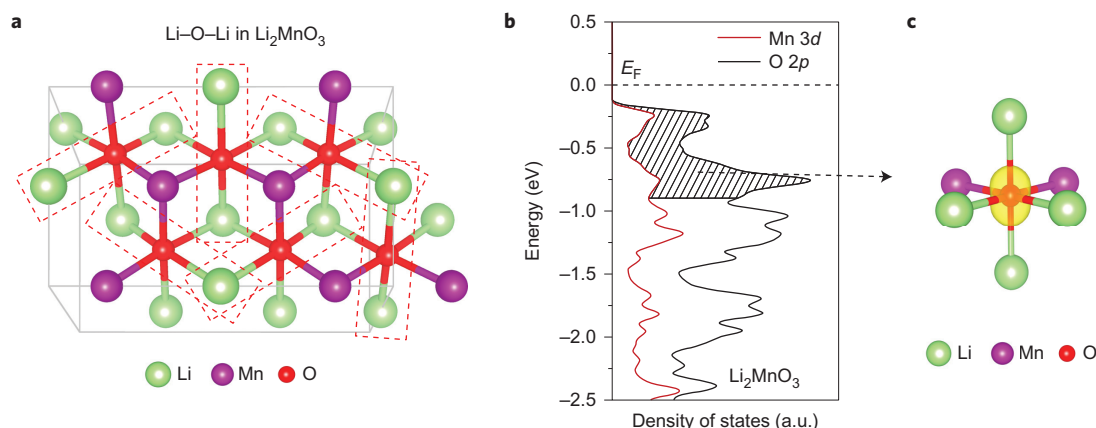
Figure 2 | Effect of Li–O–Li configurations on the electronic states of O ions in Li$_2$MnO$_3$. The Li–O–Li configurations also lead to labile oxygen states in this material. **a**, Illustration of Li–O–Li configurations in Li$_2$MnO$_3$. **b**, pDOS of the O 2p orbitals (black) and Mn 3d orbitals (red) in Li$_2$MnO$_3$. **c**, Isosurface of the charge density (yellow) around oxygen in Li$_2$MnO$_3$, in the energy range of 0 to −0.9 eV.

Li ions, in such a way that each O 2p orbital can hybridize with the M $d/s/p$ orbitals along the linear Li–O–M configuration (Fig. 4a). From here on, 'M' refers to both TM and non-TM species with d electrons. Due to the symmetry of this configuration, hybridized molecular orbitals (states) with seven different characters arise from the orbital interactions, which then form distinct bands under the periodic potential in a crystal (Fig. 4b)[10,32]. Overlap between M $3d_{x2-y2}$, d_{z2} (or 4d equivalents) and O 2p orbitals leads to e_g^b (bonding) and $e_g^\star$ (anti-bonding) states, overlap between M 4s (or 5s) and O 2p orbitals leads to a_{1g}^b (bonding) and $a_{1g}^\star$ (anti-bonding) states, and overlap between M 4p (or 5p) and O 2p orbitals leads to t_{1u}^b (bonding) and $t_{1u}^\star$ (anti-bonding) states. Finally, the overlap of the M d_{xy}, d_{yz} and d_{xz} orbitals with the O 2p orbital is negligible, which results in isolated t_{2g} states that have a non-bonding characteristic. Considering the dominant contributions in these hybridized states, the t_{2g}, $e_g^\star$, $a_{1g}^\star$ and $t_{1u}^\star$ states can be thought of as M (dominated) and the t_{1u}^b, a_{1g}^b and e_g^b states as O (dominated)[10,12,18,28,33]. This is the conventional view of the band structure of layered Li–M oxides such as LiCoO$_2$ (Fig. 4b). Because the Fermi level for the Li–M oxides lies in the $e_g^\star$ or t_{2g} band, oxidation proceeds by removing electrons from these M-dominant states. Hence, although filling or emptying an orbital near the Fermi level can cause some rehybridization and accompanying charge redistribution of the other orbitals[10], oxidation in these stoichiometric well-ordered oxides can be considered to be on the M ions (TM ions)[10,12].

However, this picture needs to be modified for other types of orbital interaction that occur in Li-excess layered or cation-disordered materials. For example, Li-excess in layered materials creates two types of O 2p orbital: the O 2p orbitals along the Li–O–M configurations and those along the Li–O–Li configurations (Fig. 4c). The O 2p orbitals along the Li–O–M configurations hybridize with the M orbitals to form the same hybridized states (bands) as in the stoichiometric layered oxides (Fig. 4b). However, those O 2p orbitals along the Li–O–Li configurations do not have an M orbital to hybridize with and do not hybridize with the Li 2s orbital either because of the large energy difference between the O 2p and Li 2s orbitals[34]. Thus, there will be orphaned unhybridized O 2p states (bands) whose density of states is proportional to the number of Li–O–Li configurations in the crystal structure (Fig. 4d).

Just as the energy levels of the t_{2g} states are close to those of unhybridized M $d_{xy}/d_{yz}/d_{xz}$ orbitals[10,32], the energy level of such an orphaned Li–O–Li state is close to that of the unhybridized O 2p orbital, putting it at a higher energy than the hybridized O bonding states (t_{1u}^b, a_{1g}^b and e_g^b states), but lower than the anti-bonding M states ($e_g^\star$, $a_{1g}^\star$ and $t_{1u}^\star$ states). The relative position of the orphaned oxygen state with respect to the non-bonding M (t_{2g}) states depends on the M species. Note that in an actual band structure there can be some overlap in energy between different states due to the broadening of the molecular-orbital energy levels under the periodic potential in the crystal structure. Therefore, competition can arise between different states (bands) upon charge transfer[35].

The preferential oxygen oxidation along the Li–O–Li configuration as observed in Fig. 3 can now be explained. As the electrons in the Li–O–Li states are higher in energy than those in the other O 2p states (Fig. 4d), oxygen oxidation preferentially occurs from the orphaned Li–O–Li states whenever Li-excess layered or cation-disordered materials are highly delithiated. Such labile Li–O–Li states in Li-excess materials may also explain why oxygen oxidation can be substantial even at a relatively low voltage of ~4.3 V in Li-excess materials[3,17,18,28].

Conditions for peroxo-like O−O bond formation. In some cases, oxygen oxidation has been claimed to result in peroxo-like species[3,36,37]. The insights presented in this Article can now be used to understand under which conditions oxygen holes can coalesce to form peroxo species and when they remain isolated. In rocksalt-like compounds where the oxygen anions form a face-centred cubic array and the cations occupy octahedral sites, oxygen p orbitals point towards the cations. The almost 90° angle between the directions of p orbitals on neighbouring oxygens prevents their σ overlap. As a result, we find that an O−O bond arises only if two neighbouring oxidized oxygens can rotate to hybridize their (oxidized) Li–O–Li states without sacrificing much M–O hybridization (Supplementary Figs 8 and 9). We find that this rotation to form peroxo-like bonds is facilitated when (1) the oxygen is bonded to a low amount of metal ions and (2) when those metal ions are not transition metals. Transition metals with partially filled d shells create strong directional bonds[38] that prevent rotation of the neighbouring oxygen bonds needed to form peroxo species. Lowering the metal coordination around oxygen, as occurs in Li-excess materials, and substituting some of the transition metals with non-transition metals, which provide weaker and less directional M–O bonds owing to the completely filled (or no) d shells, therefore facilitate peroxo-like O−O bond formation.

For example, the peroxo-like species in Li$_{0.5}$Ru$_{0.5}$Sn$_{0.5}$O$_3$ arises from σ hybridization between two neighbouring Li–O–Li states that have Li–O–Sn configurations along the other axes (Fig. 3b and Supplementary Fig. 8). In highly Li-excess materials, such O−O bond formation is therefore sometimes possible because most O ions are coordinated with at most two metal ions (Fig. 4c), so their displacement to form an O−O bond incurs less penalty. Similar effects can be expected for oxygens coordinated
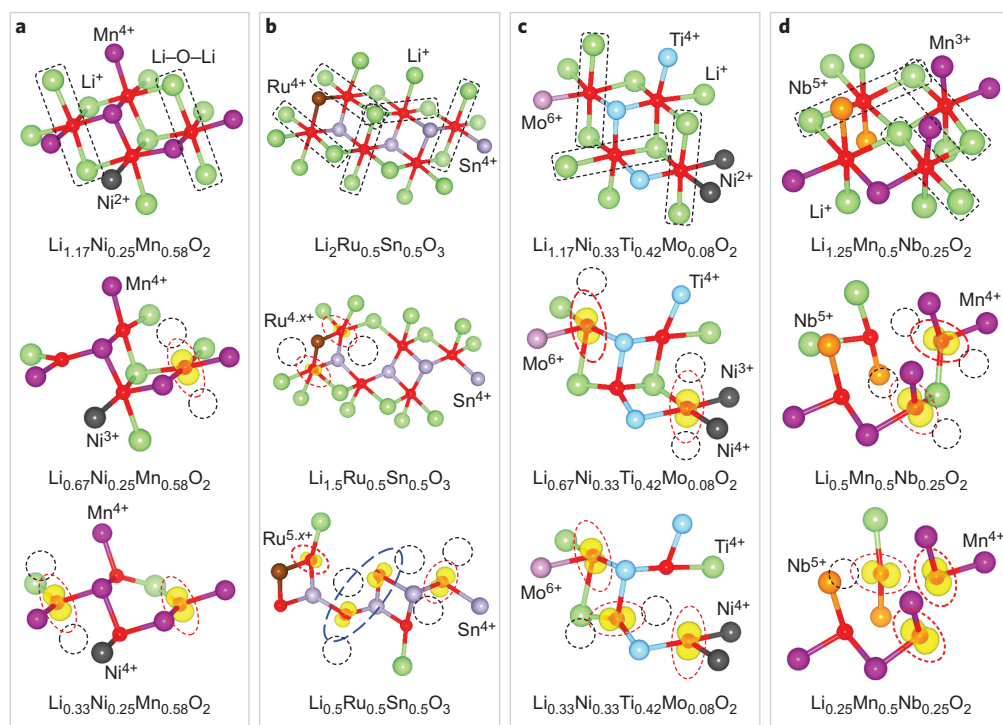
Figure 3 | Illustrations of preferred oxygen oxidation along the Li–O–Li configuration in various Li-excess materials. a–d, Atomic configuration of fully lithiated and partially delithiated Li-excess materials and the isosurface of spin density (yellow) around oxygen (red spheres) in $Li_{1.17}Ni_{0.25}Mn_{0.58}O_2$, $Li_{0.67}Ni_{0.25}Mn_{0.58}O_2$ and $Li_{0.33}Ni_{0.25}Mn_{0.58}O_2$ (**a**), in $Li_2Ru_{0.5}Sn_{0.5}O_3$, $Li_{1.5}Ru_{0.5}Sn_{0.5}O_3$ and $Li_{0.5}Ru_{0.5}Sn_{0.5}O_3$ (**b**), in $Li_{1.17}Ni_{0.33}Ti_{0.42}Mo_{0.08}O_2$, $Li_{0.67}Ni_{0.33}Ti_{0.42}Mo_{0.08}O_2$ and $Li_{0.33}Ni_{0.33}Ti_{0.42}Mo_{0.08}O_2$ (**c**) and in $Li_{1.25}Mn_{0.5}Nb_{0.25}O_2$, $Li_{0.5}Mn_{0.5}Nb_{0.25}O_2$ and $Li_{0.25}Mn_{0.5}Nb_{0.25}O_2$ (**d**). To simplify the presentation, the spin densities around metal ions are not drawn. Black dashed circles in the middle and the bottom panels indicate Li ions that have been extracted upon delithiation. In these materials, oxygen oxidation occurs preferably along the Li–O–Li configuration, which competes with transition metal oxidation. $Ru^{4.x+}$ and $Ru^{5.x+}$ in the Ru-Sn compound indicate partially oxidized Ru^{4+} and Ru^{5+}, respectively. Note that the peroxo-like species that can be observed in $Li_{0.5}Ru_{0.5}Sn_{0.5}O_3$ (blue dashed oval) arise from the σ hybridization between two neighbouring Li–O–Li states that have Li–O–Sn configurations along the other axes (Supplementary Fig. 8).

with Li–O–Li and Sb atoms along the two other directions. Oxygens in these environments satisfy all conditions for peroxo formation: (1) they are more easily oxidized due to the Li–O–Li configuration and (2) their M–O bonds rotate more easily because along the other directions, the completely filled (or no) d shells of the non-transition metals (for example, Sn and Sb) lead to a less directional M–O bond.

Therefore, peroxo-like species can form more easily in Li-excess materials containing such non-transition metals, explaining the experimental observations of peroxo-like species in $Li_2Ru_{0.5}Sn_{0.5}O_3$ or Li_4FeSbO_6 (refs 3,36). We show in Supplementary Section 'Conditions for the O–O bond formation' that such O–O bond formation depends not only on the nature of M–O hybridization, but also on the population and geometric arrangement of the oxidized Li–O–Li states (Supplementary Figs 8 and 9).

Competition between transition metal and oxygen redox. The labile electrons from the Li–O–Li states can further explain the competition between the TM redox and O redox in Li-excess materials. For example, oxidized O ions within the Li–O–Li configuration coexist with $Ru^{4.x+}$ (partially oxidized Ru^{4+}) in $Li_{1.5}Ru_{0.5}Sn_{0.5}O_3$ (Fig. 3b), indicating an overlap between the t_{2g} band (corresponding to the Ru^{4+}/Ru^{6+} redox) and the Li–O–Li band (states)[28]. Such overlap between the TM band and the Li–O–Li band is also present in $Li_{1.17-x}Ni_{0.33}Ti_{0.42}Mo_{0.08}O_2$ (ref. 30). After extracting 0.5 Li, oxidized O ions within the Li–O–Li configuration coexist with Ni^{3+} and Ni^{4+} (Fig. 3c), indicating an overlap of the Li–O–Li band and the $e_g^\star$ band (Ni^{2+}/Ni^{4+}). These results suggest that labile oxygen electrons in the Li–O–Li states

are probably the reason why some of the Li-excess layered or cation-disordered materials, such as $Li_{1.2}Ni_{0.2}Ti_{0.6}O_2$ and $Li_{1.2}Fe_{0.4}Ti_{0.4}O_2$, do not allow full TM oxidation[19,39–41]. However, overlap between the $e_g^\star$ band and the Li–O–Li band is not observed in $Li_{1.25-x}Mn_{0.5}Nb_{0.25}O_2$. As a result, oxygen oxidation only occurs after extracting more than 0.5 Li and after complete Mn^{3+} oxidation to Mn^{4+} (Fig. 3d)[40].

Because the orphaned Li–O–Li state is essentially an unhybridized O $2p$ state, its energy level remains relatively invariant with respect to changes of the structure or metal species (Supplementary Fig. 10). Hence, whether oxygen oxidation occurs before, after or simultaneously with TM oxidation depends on the energy level of the d states of different TM species. For example, both $Li_{1.17}Ni_{0.33}Ti_{0.42}Mo_{0.08}O_2$ and $Li_{1.25}Mn_{0.5}Nb_{0.25}O_2$ use TM redox from, respectively, the Ni-dominated and Mn-dominated hybridized $e_g^\star$ state. As the energy level of the Mn $3d$ orbitals is higher than that of the Ni $3d$ orbitals, the corresponding $e_g^\star$ state will also be higher in energy in $Li_{1.25}Mn_{0.5}Nb_{0.25}O_2$ than in $Li_{1.17}Ni_{0.33}Ti_{0.42}Mo_{0.08}O_2$. This reduces the overlap between the $e_g^\star$ band and the Li–O–Li band, allowing for better use of TM redox in $Li_{1.25}Mn_{0.5}Nb_{0.25}O_2$, as seems to be supported by experiments[18,29].

Based on this understanding, it seems necessary to first find the right TM species to maximize either TM redox or O redox capacity in the Li-excess materials. For example, to maximize the TM redox capacity, V, Cr, Mo or Mn can be introduced as the TM redox species. The d states of these TMs are high in energy, which raises the energy level of the $e_g^\star$ and t_{2g} bands[42]. This leads to less overlap between the TM band and the Li–O–Li band, thereby maximizing the TM redox capacity. Band overlap and thus the redox
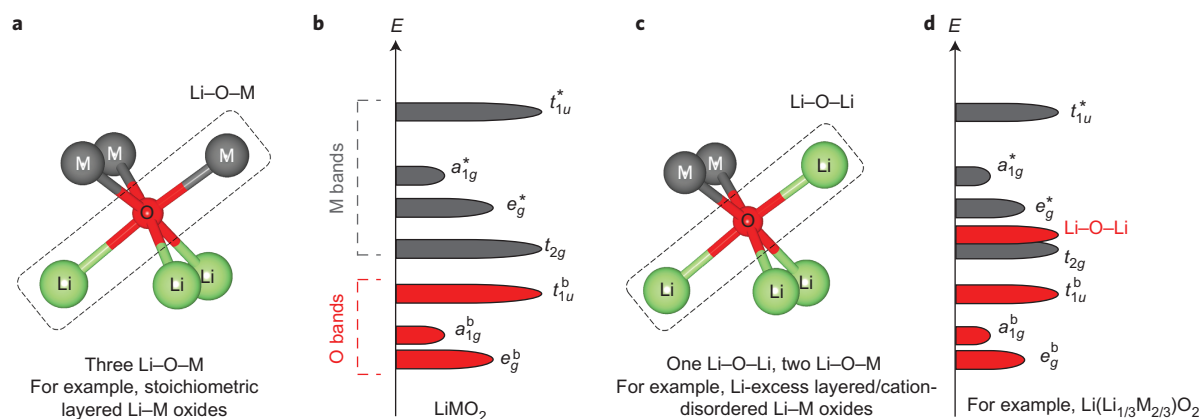
Figure 4 | Structural and chemical origin of the preferred oxygen oxidation along the Li–O–Li configuration. a, Local atomic coordination around oxygen consisting of three Li–O–M configurations in stoichiometric layered Li metal oxides (Li–M oxides). **b**, Schematic of the band structure for stoichiometric layered Li–M oxides such as LiCoO$_2$. **c**, Local atomic coordination around oxygen with one Li–O–Li and two Li–O–M configurations in Li-excess layered or cation-disordered Li–M oxides. **d**, Schematic of the band structure for Li-excess layered Li–M oxides such as Li$_2$MnO$_3$. The Li–O–Li configurations lead to unhybridized O 2p states (Li–O–Li states) whose energies are higher than those of hybridized O 2p states (t_{1u}^b, a_{1g}^b, e_g^b) and as a result are more easily oxidized.

mechanism can also be modified by engineering the lattice parameters by cation-substitution preferably with a redox-inactive metal species or by external stress through microstructure control. Modifying the lattice parameters changes the TM–O distances, which in turn alters the overlap between TM d orbitals and O 2p orbitals[10,32]. As the TM–O distance increases (decreases), the overlap between TM d orbitals and O 2p orbitals decreases (increases), so the energy level of hybridized TM d states with anti-bonding characteristic will decrease (increase) relative to the orphaned Li–O–Li states. Hence, increasing the lattice parameter should in general help to favour oxygen oxidation over TM oxidation. However, such structure manipulation needs further investigation as it might also affect other electrochemical properties or promote side reactions (for example, O loss at the surface, reactions with the electrolyte)[17,30].

In summary, we have identified the chemical and structural features that lead to oxygen oxidation and therefore to extra capacity in lithium intercalation compounds. Oxygen redox activity in Li-excess layered and disordered materials originates from very specific Li–O–Li configurations that create orphaned oxygen states that are lifted out of the bonding oxygen manifold and become positioned in the TM-dominated complex of $e_g^\star$ and t_{2g} states, making oxygen oxidation and TM oxidation compete with each other. This effect is distinct from the prevailing argument that the holes are introduced in O 2p states that are hybridized with TM d states, which occurs due to the covalent nature of the TM–O bonding[10–16]. In stark contrast with this current belief, we demonstrated that oxygen oxidation in Li-excess materials mainly occurs by extracting labile electrons from unhybridized O 2p states sitting in Li–O–Li configurations and is therefore unrelated to any hybridized TM–O states. This distinction is important, because the number of electrons, and thus the capacity, from the hybridized TM d states (for example, the $e_g^\star$ state) stays the same, regardless of the oxygen contribution to these states. Only the energy (voltage) of these TM states is modified by their hybridization[22]. Hence, unlike oxygen redox states created by Li–O–Li configurations, oxygen redox participation through (re)hybridization with TM states is not a useful mechanism to extend capacity beyond the conventional, TM-determined theoretical capacity limit.

Conclusion

Creating unhybridized (orphaned) oxygen states in Li-intercalation cathodes is a promising mechanism to achieve higher-energy-density cathode materials as it lifts the fundamental restriction on

transition metal content that has existed for decades in the Li-ion battery field. We have shown very specifically how Li-excess and cation disorder create oxygen states that compete with the transition metal states for oxidation. Although many challenges are likely to be found for such oxygen active intercalation compounds, this is an exciting new direction for the development of higher-energy-density cathode materials.

Methods

References

1. Goodenough, J. B. & Park, K.-S. The Li-ion rechargeable battery: a perspective. *J. Am. Chem. Soc.* **135,** 1167–1176 (2013).
2. Lee, J. *et al.* Unlocking the potential of cation-disordered oxides for rechargeable lithium batteries. *Science* **343,** 519–522 (2014).
3. Sathiya, M. *et al.* Reversible anionic redox chemistry in high-capacity layered-oxide electrodes. *Nature Mater.* **12,** 827–835 (2013).
4. Gallagher, K. G. *et al.* Quantifying the promise of lithium-air batteries for electric vehicles. *Energy Environ. Sci.* **7,** 1555–1563 (2014).
5. Kang, B. & Ceder, G. Battery materials for ultrafast charging and discharging. *Nature* **458,** 190–193 (2009).
6. Kang, K., Meng, Y. S., Breger, J., Grey, C. P. & Ceder, G. Electrodes with high power and high capacity for rechargeable lithium batteries. *Science* **311,** 977–980 (2006).
7. Mizushima, K., Jones, P. C., Wiseman, P. J. & Goodenough, J. B. Li$_x$CoO$_2$ ($0 \le x \le -1$): a new cathode material for batteries of high energy density. *Mater. Res. Bull.* **15,** 783–789 (1980).
8. Ohzuku, T., Ueda, A., Nagayama, M., Iwakoshi, Y. & Komori, H. Comparative study of LiCoO$_2$, LiNi$_{1/2}$Co$_{1/2}$O$_2$ and LiNiO$_2$ for 4 volt secondary lithium cells. *Electrochim. Acta* **38,** 1159–1167 (1993).
9. Lu, Z., MacNeil, D. D. & Dahn, J. R. Layered Li[Ni$_x$Co$_{1-2x}$Mn$_x$]O$_2$ cathode materials for lithium-ion batteries. *Electrochem. Solid-State Lett.* **4,** A200–A203 (2001).
10. Aydinol, M. K., Kohan, A. F., Ceder, G., Cho, K. & Joannopoulos, J. *Ab initio* study of lithium intercalation in metal oxides and metal dichalcogenides. *Phys. Rev. B* **56,** 1354 (1997).
11. Ceder, G. *et al.* Identification of cathode materials for lithium batteries guided by first-principles calculations. *Nature* **392,** 694–696 (1998).
12. Yoon, W.-S. *et al.* Oxygen contribution on Li-ion intercalation–deintercalation in LiCoO$_2$ investigated by O K-edge and Co L-edge X-ray absorption spectroscopy. *J. Phys. Chem. B* **106,** 2526–2532 (2002).

13. Yoon, W.-S. *et al.* Investigation of the charge compensation mechanism on the electrochemically Li-ion deintercalated $Li_{1-x}Co_{1/3}Ni_{1/3}Mn_{1/3}O_2$ electrode system by combination of soft and hard X-ray absorption spectroscopy. *J. Am. Chem. Soc.* **127,** 17479–17487 (2005).

14. Graetz, J. *et al.* Electronic structure of chemically-delithiated $LiCoO_2$ studied by electron energy-loss spectrometry. *J. Phys. Chem. B* **106,** 1286–1289 (2002).

15. Dahéron, L. *et al.* Electron transfer mechanisms upon lithium deintercalation from $LiCoO_2$ to CoO_2 investigated by XPS. *Chem. Mater.* **20,** 583–590 (2008).

16. Yoon, W.-S. *et al.* Combined NMR and XAS study on local environments and electronic structures of electrochemically Li-ion deintercalated $Li_{1-x}Co_{1/3}Ni_{1/3}Mn_{1/3}O_2$ electrode system. *Electrochem. Solid-State Lett.* **7,** A53–A55 (2004).

17. Koga, H. *et al.* Reversible oxygen participation to the redox processes revealed for $Li_{1.20}Mn_{0.54}Co_{0.13}Ni_{0.13}O_2$. *J. Electrochem. Soc.* **160,** A786–A792 (2013).

18. Yabuuchi, N. *et al.* High-capacity electrode materials for rechargeable lithium batteries: Li_3NbO_4-based system with cation-disordered rocksalt structure. *Proc. Natl Acad. Sci. USA* **112,** 7650–7655 (2015).

19. Goodenough, J. B. & Kim, Y. Challenges for rechargeable Li batteries. *Chem. Mater.* **22,** 587–603 (2010).

20. Kohn, W. & Sham, L. J. Self-consistent equations including exchange and correlation effects. *Phys. Rev.* **140,** A1133 (1965).

21. Heyd, J., Scuseria, G. E. & Ernzerhof, M. Hybrid functionals based on a screened Coulomb potential. *J. Chem. Phys.* **118,** 8207–8215 (2003).

22. Seo, D.-H., Urban, A. & Ceder, G. Calibrating transition metal energy levels and oxygen bands in first principles calculations: accurate prediction of redox potentials and charge transfer in lithium transition metal oxides. *Phys. Rev. B* **92,** 115118 (2015).

23. Ohzuku, T. & Makimura, Y. Layered lithium insertion material of $LiCo_{1/3}Ni_{1/3}Mn_{1/3}O_2$ for lithium-ion batteries. *Chem. Lett.* **30,** 642–643 (2001).

24. Cho, Y. & Cho, J. Significant improvement of $LiNi_{0.8}Co_{0.15}Al_{0.05}O_2$ cathodes at 60 °C by SiO_2 dry coating for Li-ion batteries. *J. Electrochem. Soc.* **157,** A625–A629 (2010).

25. Lu, Z. H., MacNeil, D. D. & Dahn, J. R. Layered cathode materials $Li[Ni_xLi_{(1/3-2x/3)}Mn_{(2/3-x/3)}]O_2$ for lithium-ion batteries. *Electrochem. Solid-State Lett.* **4,** A191–A194 (2001).

26. Xiao, R., Li, H. & Chen, L. Density functional investigation on Li_2MnO_3. *Chem. Mater.* **24,** 4242–4251 (2012).

27. Lee, E. & Persson, K. A. Structural and chemical evolution of the layered Li-excess Li_xMnO_3 as a function of Li content from first-principles calculations. *Adv. Energy Mater.* **4,** 1400498 (2014).

28. Sathiya, M. *et al.* High performance $Li_2Ru_{1-y}Mn_yO_3$ ($0.2 \leq y \leq 0.8$) cathode materials for rechargeable lithium-ion batteries: their understanding. *Chem. Mater.* **25,** 1121–1131 (2013).

29. Wang, R. *et al.* A new disordered rock-salt Li-excess material with high capacity: $Li_{1.25}Nb_{0.25}Mn_{0.5}O_2$. *Electrochem. Commun.* **60,** 70–73 (2015).

30. Lee, J. *et al.* A new class of high capacity cation-disordered oxides for rechargeable lithium batteries: Li-Ni-Ti-Mo oxides. *Energy Environ. Sci.* **8,** 3255–3265 (2015).

31. Petersburg, C. F., Li, Z., Chernova, N. A., Whittingham, M. S. & Alamgir, F. M. Oxygen and transition metal involvement in the charge compensation mechanism of $LiNi_{1/3}Mn_{1/3}Co_{1/3}O_2$ cathodes. *J. Mater. Chem.* **22,** 19993–20000 (2012).

32. Ballhausen, C. J. *Ligand Field Theory* (McGraw Hill, 1962).

33. Oishi, M. *et al.* Charge compensation mechanisms in $Li_{1.16}Ni_{0.15}Co_{0.19}Mn_{0.50}O_2$ positive electrode material for Li-ion batteries analyzed by a combination of hard and soft X-ray absorption near edge structure. *J. Power Sources* **222,** 45–51 (2013).

34. Pauling, L. *The Nature of the Chemical Bond* Vol. 3 (Cornell Univ. Press, 1960).

35. Ashcroft, N. W. & Mermin, N. D. *Solid State Physics* 490–495 (Holt, Rinehart and Winston, 1976).

36. McCalla, E. *et al.* Understanding the roles of anionic redox and oxygen release during electrochemical cycling of lithium-rich layered Li_4FeSbO_6. *J. Am. Chem. Soc.* **137,** 4804–4814 (2015).

37. Saubanere, M., McCalla, E., Tarascon, J. M. & Doublet, M. L. The intriguing question of anionic redox in high-energy density cathodes for Li-ion batteries. *Energy Environ. Sci.* **9,** 984–991 (2016).

38. Morrison, S. *The Chemical Physics of Surfaces* (Springer, 2012).

39. Zhang, L. *et al.* Synthesis and electrochemistry of cubic rocksalt Li–Ni–Ti–O compounds in the phase diagram of $LiNiO_2$–$LiTiO_2$–$Li[Li_{1/3}Ti_{2/3}]O_2$. *J. Power Sources* **185,** 534–541 (2008).

40. Shigemura, H., Tabuchi, M., Sakaebe, H., Kobayashi, H. & Kageyama, H. Lithium extraction and insertion behavior of nanocrystalline Li_2TiO_3–$LiFeO_2$ solid solution with cubic rock salt structure. *J. Electrochem. Soc.* **150,** A638–A644 (2003).

41. Glazier, S. L., Li, J., Zhou, J., Bond, T. & Dahn, J. R. Characterization of disordered $Li_{(1+x)}Ti_{2x}Fe_{(1-3x)}O_2$ as positive electrode materials in Li-ion batteries using percolation theory. *Chem. Mater.* **27,** 7751–7756 (2015).

42. Lias, S. Ionization energy search, *NIST chemistry webbook, NIST standard reference database 69* (2005); http://webbook.nist.gov/chemistry/ie-ser.html

43. Kresse, G. & Furthmuller, J. Efficiency of *ab-initio* total energy calculations for metals and semiconductors using a plane-wave basis set. *Comput. Mater. Sci.* **6,** 15–50 (1996).

Author contributions
G.C. planned the project, supervised all aspects of the research, contributed to the main theory and to writing the manuscript. D.-H.S. and J.L. conceived and designed project details. D.-H.S. performed DFT calculations. D.-H.S. and J.L. analysed the data. J.L. and D.-H.S. developed the main theory and authored the manuscript. D.-H.S and J.L. contributed equally to this work. A.U. and S.Y.K. performed preliminary DFT calculations. A.U. and R.M. assisted in data analysis and in writing the manuscript.

Additional information
Supplementary information is available in the online version of the paper. Reprints and permissions information is available online at www.nature.com/reprints. Correspondence and requests for materials should be addressed to G.C.

Competing financial interests
The authors declare no competing financial interests.